

Article

Enhancement of Ni Catalyst Using CeO₂–Al₂O₃ Support Prepared with Magnetic Inducement for ESR

Pumiwat Vacharapong¹, Sirintra Arayawate¹, Sasimas Katanyutanon¹, Pisanu Toochinda^{1,*}, Luckhana Lawtrakul^{1,*}  and Sumittra Charojrochkul²

¹ School of Bio-Chemical Engineering and Technology (BCET), Sirindhorn International Institute of Technology (SIIT), Thammasat University, Pathum Thani 12120, Thailand; pumiwat.v@gmail.com (P.V.); sirintra.ara@gmail.com (S.A.); por.katanyutanon@gmail.com (S.K.)

² National Energy Technology Center (ENTEC), National Science and Technology Development Agency (NSTDA), Pathum Thani 12120, Thailand; sumittra.cha@entec.or.th

* Correspondence: pisanu@siit.tu.ac.th (P.T.); luckhana@siit.tu.ac.th (L.L.)

Received: 4 November 2020; Accepted: 19 November 2020; Published: 21 November 2020



Abstract: The effect of magnetic inducement in support preparation was studied to reduce coke and improve the activity of Ni catalysts for ethanol steam reforming (ESR) at 550–650 °C. Magnetic inducement was introduced to prepare 5 mol % CeO₂ in Al₂O₃ support in order to control the composition and the distribution of Ce in Al₂O₃. The results show that using CeO₂–Al₂O₃ support with magnetic inducement affects both hydrogen production and coke reduction, where Ni/CeO₂–Al₂O₃ support prepared under magnetic inducement with N–N pole arrangement (Ni/CeO₂–Al₂O₃ (N–N)) exhibited the highest hydrogen production and the lowest coke formation among the catalysts used in this work. Compared with Ni/CeO₂–Al₂O₃ (no magnet), Ni/CeO₂–Al₂O₃ (N–N) catalysts yield 14.0% higher H₂ production and 31.7% less coke production. The modified catalyst preparation process used in this study could create catalysts for hydrogen production from ESR which are high in performance and stability but low in preparation cost.

Keywords: supported catalysts; magnetic inducement; coke reduction; support modification

1. Introduction

Ethanol steam reforming (ESR) is one of the reforming reactions of hydrocarbon to produce H₂, which is considered as a renewable energy source due to ethanol production from biomass fermentation. ESR pathways comprise many reaction routes [1]. However, the most preferable is the main reaction which yields up to six moles of H₂ per mole of ethanol, as shown in Equation (1).



Coking is a long-term catalyst deactivation due to carbon deposition overactive metal sites during a reaction which commonly occurs in hydrocarbon reforming [2–5]. An appropriate catalyst for ESR promotes the main reaction over the side reactions that produce CO, which is a coke precursor. The best catalysts for ESR reported in the literature are Rh-based catalysts which are active at 600 °C with low coking [6–8]. However, the high cost and the low availability of Rh exponentially increases the cost of H₂ production from ESR. In order to reduce the cost, investigations of other metals to replace Rh are widely studied. The literature reports that among non-noble metal catalysts (Cu, Zn, Co, Ni), Ni exhibits the highest activity for ESR [6,9]. However, Ni-based catalysts can suffer from deactivation due to coking at reaction temperatures as low as 500 °C at certain reaction conditions [10]. Additional cost is required to remove the coke and reactivate the catalysts via calcination with air and

reduction with H_2 , respectively. Therefore, coking is the main drawback of Ni catalysts to serve as a substitution of Rh catalysts for ESR at low temperatures. The development of Ni catalysts that are active at low operating temperature and exhibit low coke formation is required. An approach to solve this problem is to increase Ni dispersion on the catalyst and investigate the support to reduce coke formation for ESR at low temperature.

Ceria has been reported as a support that can reduce the coke formation for reforming of hydrocarbons due to its high oxygen storage capacity [11–16]. Oxygen storage capacity of CeO_2 is essential in retaining oxygen gas (O_2) which is used to remove the carbon residue on the metal active sites [17,18]. However, the cost of CeO_2 is particularly high to use solely as the support, and the low surface area of CeO_2 is also not suitable for serving as a support for heterogeneous catalysts. Therefore, partial doping of CeO_2 to Al_2O_3 should yield a support with high surface area with the benefit of coke reduction property. Doping CeO_2 into Al_2O_3 also results in the creation of an oxygen vacancies. Oxygen vacancies can serve as nucleation sites for metal clusters [19]. Therefore, dispersion of CeO_2 on Al_2O_3 framework surface should affect Ni dispersion on the support.

The literature reported that applying an external magnetic field to a dilute solution can cause ions to move differently during gelation process [20]. Therefore, magnetic inducement is introduced in an attempt to control the composition and the distribution of Ce in Al_2O_3 framework during the sol-gel process in order to improve the homogeneity of the dopant in the support framework. This work aimed to increase the activity of Ni catalysts at low temperatures and reduce coking, which was accomplished by support modification of CeO_2 partial doping into an Al_2O_3 framework with magnetic inducement. This support modification provides an attractive development of a low-cost Ni catalyst which is active at low temperature and able to reduce coking for H_2 production from ESR.

2. Results

2.1. Effect of CeO_2 – Al_2O_3 Support Prepared with and without Magnetic Inducement

2.1.1. Effect on H_2 , CO_2 and CO Production

ESR occurs together with other side reactions. The main products of ESR are H_2 and CO_2 , while CO is a byproduct from methane reforming and decomposition of acetaldehyde which is more likely to convert to coke compared to CO_2 [21]. Therefore, the rate of H_2 production and the CO_2 :CO ratio can give information regarding the preferred pathway.

Table 1 shows the H_2 , CO_2 and CO production rate with the CO_2 :CO ratio from ESR over Ni/ γ - Al_2O_3 and Ni/ CeO_2 - Al_2O_3 with and without magnetic inducement at 550 °C and 650 °C in continuous mode, respectively. The results show that doping Ce into an Al_2O_3 framework and using it as a support helps in the H_2 production rate of the Ni catalyst. By doping Ce into an Al_2O_3 framework and implementing a magnet (N–N and S–S) during support preparation, Ni/ CeO_2 - Al_2O_3 (N–N), Ni/ CeO_2 - Al_2O_3 (S–S) catalysts yielded a higher H_2 production rate and CO_2 :CO than the other catalysts at both temperatures. A trace of CH_4 was detected only at 550 °C in the range of 2.4–3.6 mmol/min·g_{cat}, but none was found at 650 °C. Ethylene was not found in the product stream in the operating temperature range. The result of the CO_2 and CO production rate confirms that the catalyst which exhibited higher H_2 production also yielded a higher ratio of CO_2 :CO, implying that ESR was the preferred pathway in the process.

Table 1. H₂ production rate of Ni catalysts at 550 and 650 °C.

Catalysts	Gaseous Production Rate (mmol/min·g _{cat})								
	Temperature	550 °C				650 °C			
		H ₂	CO ₂	CO	CO ₂ :CO	H ₂	CO ₂	CO	CO ₂ :CO
Ni/γ-Al ₂ O ₃	672.1 ± 1.6	235.7	37.9	6.21	683.4 ± 5.7	231.0	71.0	3.27	
Ni/CeO ₂ -Al ₂ O ₃	680.1 ± 2.1	258.3	41.2	6.27	761.9 ± 2.8	276.7	38.8	7.13	
Ni/CeO ₂ -Al ₂ O ₃ (N-S)	675.1 ± 3.6	255.0	39.1	6.52	727.7 ± 4.3	238.8	32.8	6.94	
Ni/CeO ₂ -Al ₂ O ₃ (N-N)	773.2 ± 4.2	293.9	41.6	7.07	885.8 ± 5.4	336.3	24.9	9.13	
Ni/CeO ₂ -Al ₂ O ₃ (S-S)	781.5 ± 3.3	299.5	37.2	8.06	813.6 ± 4.8	299.3	28.3	8.04	

2.1.2. Effect on Coke Reduction

Table 2 shows the amount of coke produced over Ni catalysts after the ESR process in this study, determined using Temperature Program Oxidation (TPO) technique at 550, 650 and 750 °C. In addition, the coke production at 750 °C was determined in order to observe a clear difference in the coke reduction capability of the prepared catalysts. The data shows that catalysts on CeO₂-Al₂O₃ support contained a lower coke content than that over γ-Al₂O₃, because Ce can provide oxygen to gasify the deposited carbon and subsequently prevent coking. Magnetic inducement and pole arrangement also affected the coke reduction in the catalysts. Ni/CeO₂-Al₂O₃ prepared under same magnetic pole (N-N) and (S-S) exhibited the highest coke reduction. On the other hand, Ni/CeO₂-Al₂O₃ (N-S) showed poor coke reduction, even outperformed by Ni/CeO₂-Al₂O₃ prepared without magnetic inducement. This trend correlates negatively with the CO₂:CO ratio reported in Table 1, where a higher CO₂:CO ratio corresponds with lower amounts of coke formed.

The reduced coke formation from Ni/CeO₂-Al₂O₃ prepared without magnetic inducement is due to oxygen vacancies from the CeO₂ dopant which provides oxygen to gasify the deposited carbons to CO₂. The increase in CO₂ production can drive the Boudouard reaction (Equation (2)) backward, causing a decrease in coke formation.



However, magnetic inducement with proper pole arrangements can significantly reduce the coke formation. In order to understand the role of magnetic inducement on Ce dopants in Al₂O₃ framework and on coke reduction on Ni catalysts, the following characterizations: XRD, Brunauer, Emmett and Teller (BET) surface analysis, and SEM-EDS, were performed.

Table 2. Coke formation over Ni catalysts.

Catalysts	Coke (mg/g _{cat})		
	550 °C	650 °C	750 °C
Ni/γ-Al ₂ O ₃	1.46	2.41	4.97
Ni/CeO ₂ -Al ₂ O ₃	1.32	2.13	4.08
Ni/CeO ₂ -Al ₂ O ₃ (N-S)	1.42	2.28	4.84
Ni/CeO ₂ -Al ₂ O ₃ (N-N)	1.25	1.71	2.82
Ni/CeO ₂ -Al ₂ O ₃ (S-S)	1.30	1.75	2.79

2.1.3. Stability Test

Figure 1 shows the H₂ production at 650 °C from Ni/γ-Al₂O₃ and Ni/CeO₂-Al₂O₃ (N-N) which exhibited the lowest and highest catalytic activity among the catalysts used, respectively. The stability test was run for 30 h. The result shows that while the H₂ production from Ni/γ-Al₂O₃ started to drop after 5 h of reaction, Ni/CeO₂-Al₂O₃ (N-N) achieved a higher H₂ production rate with lower decrease rate for 30 h. Therefore, the amount of coke is directly related to the deactivation of the catalyst, which corresponds to the results in Table 2.

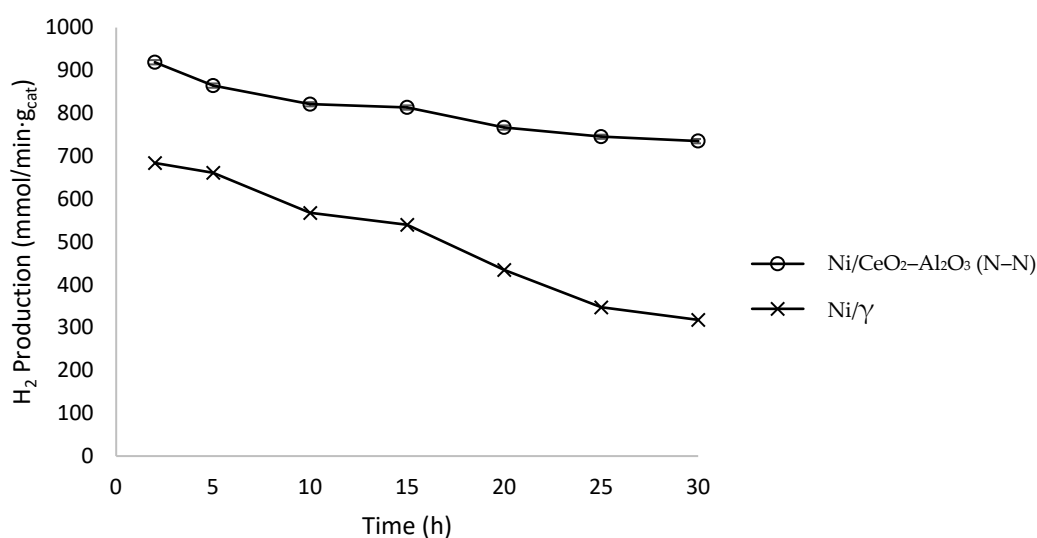


Figure 1. H₂ production from Ni/γ-Al₂O₃ and Ni/CeO₂-Al₂O₃ (N-N) at 650 °C.

2.2. Catalyst and Support Characterization

Table 3 lists the Ni content, dispersion percentage, and surface areas of the catalysts in this study. Ni contents of the catalysts were determined using the inductively coupled plasma optical emission spectrometry (ICP-OES) technique. The results show the same range of Ni contents in each catalyst (from 9.60 ± 0.13 to 9.86 ± 0.20 wt %). This ensures that the catalytic activity of Ni catalysts is based on the same Ni mass basis in this study. The results also show that doping Ce into the Al₂O₃ framework enhances both the dispersion and the surface area of Ni active sites. Ce dopants cause defects in the Al₂O₃ framework and serve as nucleation points for Ni atoms [20]. Magnetic inducement clearly affects the Ni dispersion on this support. Ni/CeO₂-Al₂O₃ catalysts prepared under same pole magnetic inducements (N-N and S-S) exhibit the highest Ni surface area and Ni dispersion. In contrast, Ni/CeO₂-Al₂O₃ (N-S) does not show any changes in these properties compared to Ni catalyst on the support prepared without magnetic inducement. These differences in Ni dispersion and surface area are due to the effect of magnetic inducement on the insertion of Ce into the Al₂O₃ framework.

Table 3. Ni content, Ni dispersion and Ni surface area of catalysts.

Catalysts	Ni Content (wt %)	Ni Dispersion (%)	Ni Surface Area (m ² /g _{Ni})
Ni/γ-Al ₂ O ₃	9.70 ± 0.15	1.0	7.3
Ni/CeO ₂ -Al ₂ O ₃	9.60 ± 0.13	2.8	18.3
Ni/CeO ₂ -Al ₂ O ₃ (N-S)	9.82 ± 0.19	2.9	18.8
Ni/CeO ₂ -Al ₂ O ₃ (N-N)	9.86 ± 0.20	3.2	21.4
Ni/CeO ₂ -Al ₂ O ₃ (S-S)	9.62 ± 0.19	3.2	21.0

Table 4 lists physical properties of the supports in this study including the surface areas, the average pore diameters, and the lattice constants. The lattice constants obtained from XRD pattern analysis of CeO₂-Al₂O₃ supports in Figure 2 were different from those of Al₂O₃, which was caused by the defect and the distortion of the Al₂O₃ structure due to the doped Ce atoms [8]. The change in the unit cell of Al₂O₃ structure led to larger lattice constants in CeO₂-Al₂O₃. A larger lattice constant implies better Ce insertion into the Al₂O₃ framework [16], thus the supports prepared with N-N and S-S magnetic pole arrangement showed better Ce insertion than the support prepared without magnetic inducement and with N-S magnetic pole arrangement.

All CeO₂-Al₂O₃ supports had surface areas lower than that of Al₂O₃. The decrease in support surface area comes from the high proportion of Ce, which has a surface area lower than that of Al₂O₃ [22]. The supports prepared under the same pole magnetic inducement (N-N and S-S) yielded

lower surface areas than the support with opposite pole inducement (N–S). The results imply that there are more Ce atoms in the Al_2O_3 framework when the support is prepared under the same pole magnetic inducement, corresponding with the implication from the lattice constants.

Table 4. Physical properties of $\gamma\text{-Al}_2\text{O}_3$ and $\text{CeO}_2\text{-Al}_2\text{O}_3$ supports.

Supports	Preparation Method		Surface Area (m^2/g)	Pore Volume (cm^3/g)	Average Pore Diameter (\AA)	Lattice Constant of Al_2O_3 Framework (\AA)
	Process	Magnetic Inducement				
$\gamma\text{-Al}_2\text{O}_3$	Sol-gel	none	165.3	0.39	95.1	7.9068
		none	138.1	0.33	94.3	7.9141
$\text{CeO}_2\text{-Al}_2\text{O}_3$	Sol-gel	N–S	142.2	0.32	91.2	7.9145
		N–N	135.6	0.33	96.3	7.9220
		S–S	135.6	0.32	94.2	7.9180
		S–S	135.6	0.32	94.2	7.9180

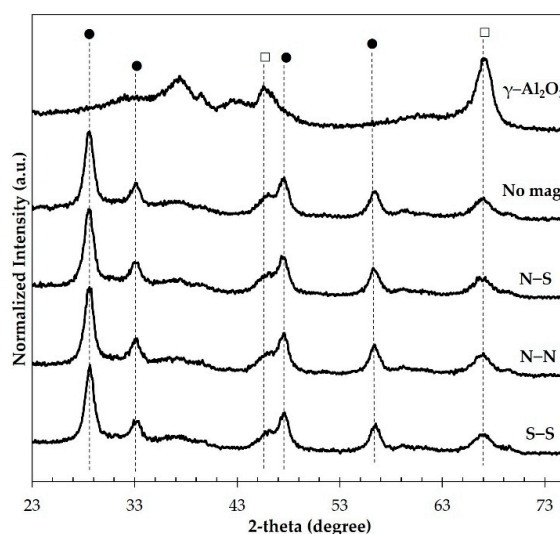


Figure 2. XRD patterns of $\gamma\text{-Al}_2\text{O}_3$ and $\text{CeO}_2\text{-Al}_2\text{O}_3$ prepared with and without magnetic inducement supports, \square : face centered cubic Al_2O_3 , \bullet : face centered cubic CeO_2 .

Therefore, magnetic inducement with certain pole arrangements might be able to control the Ce composition in the Al_2O_3 framework during the support preparation by the sol-gel process.

The SEM-EDS technique was used to identify the Ce distribution on the surface of the $\text{CeO}_2\text{-Al}_2\text{O}_3$ support by random sampling at different points. The SEM-EDS data were collected from five random particles of each support, measured at three points on each particle, to visualize the Ce distribution on the surfaces of $\text{CeO}_2\text{-Al}_2\text{O}_3$ supports and determine the range of Ce compositions in the Al_2O_3 framework.

The Ce compositions are represented in term of the molar ratio of Ce:Al, as listed in Table 5. The doped support without magnetic inducement showed a wide range of Ce composition with high standard deviation, which implies that Ce is randomly inserted into the Al_2O_3 framework. Therefore, the magnetic inducement during sol-gel preparation can uniformly distribute Ce into the Al_2O_3 framework, resulting in a narrower Ce:Al ratio range with a low standard deviation.

Table 5. Compositions in terms of Ce:Al molar ratio of $\text{CeO}_2\text{-Al}_2\text{O}_3$ supports with and without magnetic inducement.

Supports	Magnetic Inducement	Ce:Al Molar Ratio $\times 10^2$		
		Range	Average	SD
$\text{CeO}_2\text{-Al}_2\text{O}_3$	none	4.32–26.17	9.65	9.28
	N–S	2.00–2.66	2.38	0.29
	N–N	7.20–7.98	7.58	0.33
	S–S	6.24–7.09	6.70	0.35

The application of the same magnetic pole arrangement (N–N and S–S) yielded the highest Ce:Al molar ratio and the best Ce distribution in the Al_2O_3 framework. On the contrary, the application of an opposing magnetic pole arrangement (N–S) yielded the lowest Ce:Al molar ratio, even lower than the support prepared without magnetic inducement. This corresponds to and confirms the results from the BET surface area and the lattice constants of the supports, which suggest that same magnetic pole arrangements yield the best Ce insertion into the Al_2O_3 framework.

The addition of Ce dopants not only improves Ni dispersion on the support, but also creates oxygen vacancies to react with carbon species formed on the catalysts after long-term use. Improvement of Ce composition and distribution in the Al_2O_3 framework thus directly affects the H_2 production and the amount of coke formed. The application of magnetic inducement during the support preparation, as reported elsewhere, causes Ce^{3+} and Al^{3+} ions to move differently, especially for the same magnetic pole arrangement [23]. The magnetic field gradient produced between same magnetic poles, as shown in Figure 3, can drive paramagnetic ions, such as Ce^{3+} ions, to move towards regions with stronger magnetic field. On the other hand, diamagnetic ions, such as Al^{3+} ions, are generally less affected by magnetic fields. Application of a magnetic field to a dilute aqueous solution also leads to higher viscosity. The decrease in Ce dispersion in the Al_2O_3 framework in the support prepared under opposite magnetic pole arrangement is a probable result of the higher viscosity of the Ce–Al solution. In contrast, a same magnetic pole arrangement provides extra driving force for movements of Ce^{3+} ions, causing them to better disperse into regions rich in Al^{3+} ions.

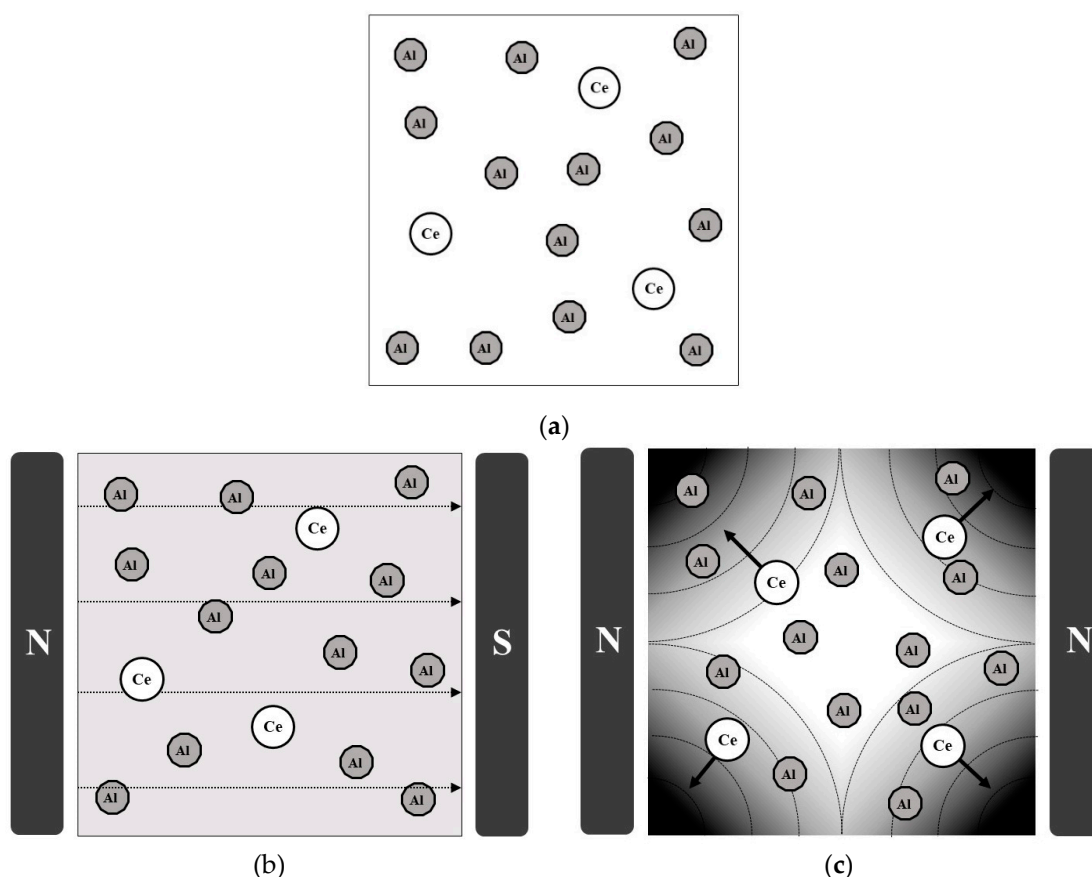


Figure 3. Schematic of Ce^{2+} and Al^{3+} movement under (a) no magnetic inducement (b) magnetic field from opposite magnetic pole arrangement (N–S) and (c) same magnetic pole arrangement (N–N or S–S).

The XPS spectra of Ni 2p on CeO₂–Al₂O₃ supports are shown in Figure 4. The spectra exhibit characteristic peaks of NiO at 854 and 871 eV. The peaks of Ni₂O₃ or NiAl₂O₄ are observed at binding energies of 856 and 873 eV, respectively. The lack of observable peak shift for Ni 2p between Ni catalysts loaded onto CeO₂–Al₂O₃ prepared with and without magnetic inducement suggests that magnetic inducement does not affect the oxidation states of Ni active metal.

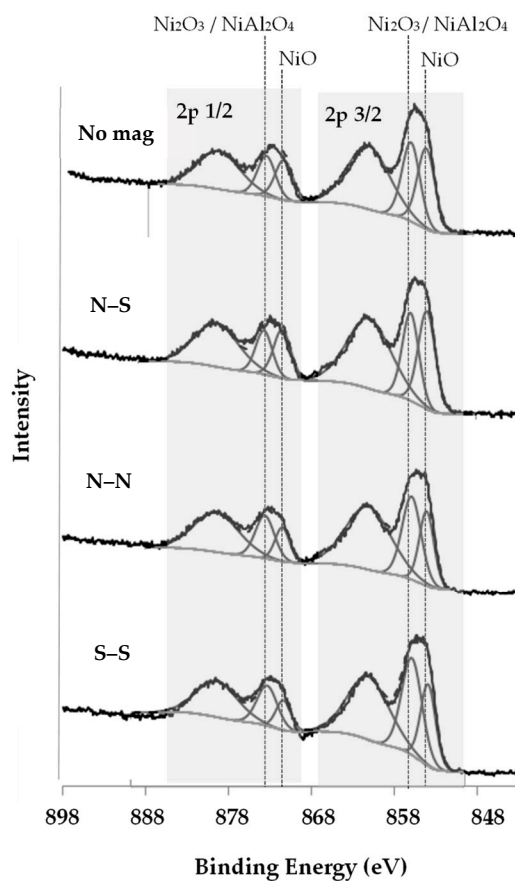


Figure 4. Ni 2p XPS spectrograms of Ni/CeO₂–Al₂O₃ prepared with and without magnetic inducement.

In order to determine the oxidation states of Al and Ce, the Al₂O₃ and CeO₂–Al₂O₃ supports were also analyzed with XPS spectrometry. The XPS spectra of Al 2p and Ce 3d are presented in Figures 5 and 6, respectively, with the list of characteristic peaks presented in Table 6.

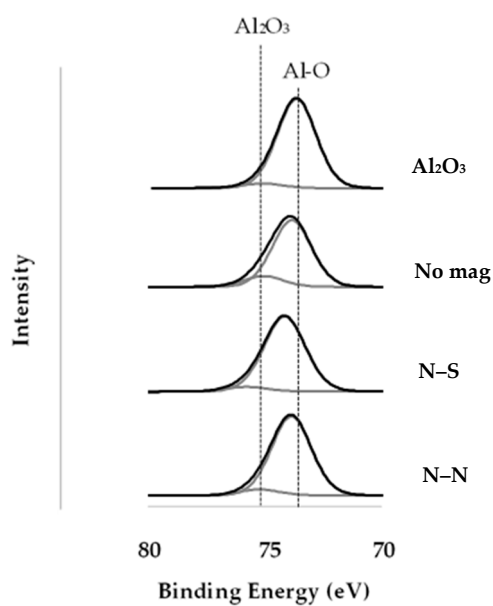


Figure 5. Al 2p XPS spectrograms of Al₂O₃ and CeO₂-Al₂O₃ prepared with and without magnetic inducement.

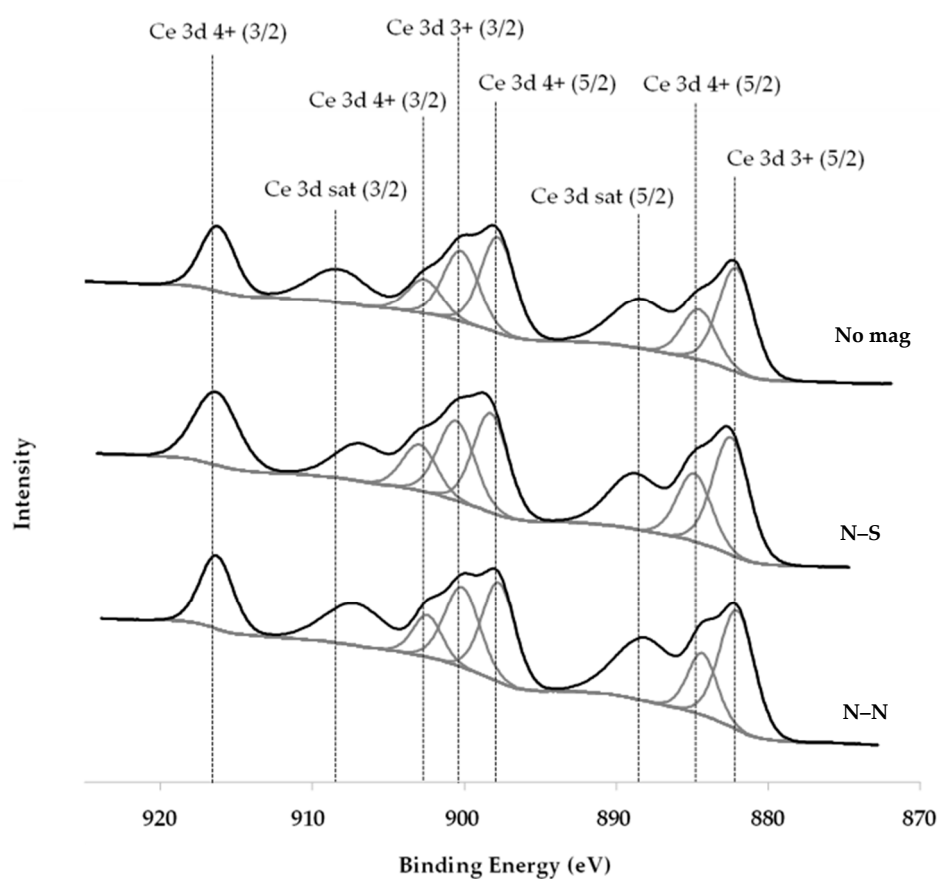


Figure 6. Ce 3d XPS spectrograms of CeO₂-Al₂O₃ prepared with and without magnetic inducement.

Table 6. Peak energy of Al 2p and Ce 3d XPS spectrograms.

Support	Peak Energy (eV)									
	Al–O	Al ₂ O ₃	Ce 3d (3+) 5/2	Ce 3d (3+) 3/2	Ce 3d (4+) 5/2	Ce 3d (4+) 3/2	Ce 3d (sat) 5/2	Ce 3d (sat) 3/2		
γ -Al ₂ O ₃	73.64	75.08	-	-	-	-	-	-		
CeO ₂ -Al ₂ O ₃	73.84	75.06	882.12	900.22	884.53	897.79	902.63	916.23	888.36	908.31
CeO ₂ -Al ₂ O ₃ (N-S)	74.15	75.77	882.44	900.54	884.85	898.26	902.95	916.36	888.73	906.83
CeO ₂ -Al ₂ O ₃ (N-N)	73.86	75.23	882.04	900.14	884.33	897.73	902.43	916.31	888.07	907.20

In Figure 5 and Table 6, differences are observed in Al 2p binding energy between Al₂O₃ and CeO₂-Al₂O₃ supports prepared with and without magnetic inducement. The Al–O peak was slightly shifted to the higher binding energy side when Ce was doped to the Al₂O₃ support. In Figure 6 and Table 6, Ce 3d peak energy also showed a similar pattern with slight peak shift on Ce 3d sat (3/2). However, the distribution of Ce³⁺ and Ce⁴⁺ cannot be defined, because XPS experimentation was executed under vacuum conditions without O₂. Therefore, there is no solid explanation for this phenomenon, but this result might be useful for further investigation with other techniques.

Therefore, the application of magnetic inducement during CeO₂-Al₂O₃ support preparation does not cause significant differences in the oxidation states of Al and Ce. Magnetic inducement affects only the distribution and composition of Ce in Al₂O₃. The defects due to oxygen vacancies in CeO₂ serve as nucleation points for Ni [22], therefore a higher composition of Ce on the surface of the Al₂O₃ framework leads to better dispersion of Ni, as supported by the results from CO pulse chemisorption. Magnetic inducement with the same magnetic pole arrangement during CeO₂-Al₂O₃ support preparation thus improves the catalytic activity of Ni catalysts by creating a larger number of Ni active sites without significantly changing the reaction pathway and the electronic structure of the catalyst.

3. Conclusions

From this study, we discovered that by introducing magnetic inducement using different pole arrangements (N–N, S–S, and N–S) during the CeO₂-Al₂O₃ support preparation, the surface areas of the supports can be altered. There is, thus, a possibility that magnetic inducement can be used to control the composition of the doped Ce in Al₂O₃ supports due to its effect on the viscosity of the metal solution and the movement of paramagnetic Ce²⁺ ions. The supports prepared under the same pole magnetic inducement (N–N and S–S) yielded a lower surface area than that of the support with opposite pole inducement (N–S) due to a higher Ce composition in the Al₂O₃ framework. After impregnation, Ni/CeO₂-Al₂O₃ (N–N) and Ni/CeO₂-Al₂O₃ (S–S) catalysts exhibited the highest Ni surface area and Ni dispersion which corresponded to the highest H₂ production rate and the highest CO₂:CO ratio at 550 °C and 650 °C. The higher Ce composition in Ni/CeO₂-Al₂O₃ (N–N) and Ni/CeO₂-Al₂O₃ (S–S) catalysts also related to a lower coke formation as expected, due to the oxygen storage capacity of Ce.

4. Materials and Methods

4.1. Support Preparation

The CeO₂-Al₂O₃ supports were prepared with 5 mol % of dopant following these steps. Ce(NO₃)₃·6H₂O (≥99%, Fluka, North Carolina, USA) and Al(NO₃)₃·9H₂O (≥98%, LOBA Chemie, Mumbai, India) were separately dissolved in deionized water to form 0.1 M salt solutions. The Ce salt solution was mixed with Al salt solution to form a Ce–Al salt solution with a mole ratio of 0.1:9.9. Ammonia solution (30 vol %, Panreac AppliChem, Darmstadt, Germany) was dropped into the mixed salt solutions to form gel until the pH of the salt solution reached 9 within 60 min with the influence of

a magnetic field as shown in Figure 7 (same poles and opposite poles), and without. The Ce–Al gels were kept at room temperature for 48 h and dried at 110 °C for 24 h. The dried gels were calcined at 800 °C for 4 h to obtain CeO₂–Al₂O₃, CeO₂–Al₂O₃ (N–S), CeO₂–Al₂O₃ (N–N) and CeO₂–Al₂O₃ (S–S) supports. The undoped γ -Al₂O₃ was prepared with the same preparation procedure as the CeO₂–Al₂O₃ support without magnetic inducement. All supports were ground and sieved using 106 μ m sieves to control the support particle size.

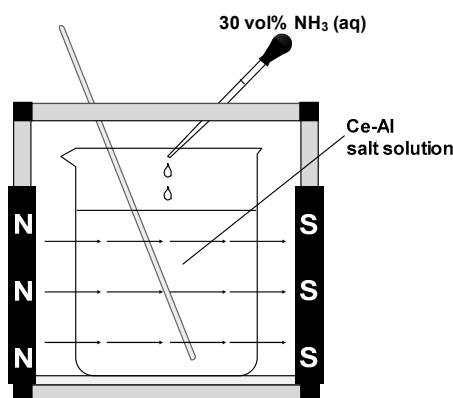


Figure 7. Magnetic setup for magnetic inducement (N–S).

4.2. Catalyst Preparation

The 10 wt % of Ni catalysts were prepared using an incipient wetness impregnation method. Ni(NO₃)₂·6H₂O ($\geq 99\%$, LOBA Chemie, Mumbai, India) with 2 mol of urea was dissolved in deionized water to obtain Ni solutions with a concentration of 1.25 M. The Ni solutions were impregnated over the supports. After impregnation, the catalysts were dried at 110 °C for 12 h and then calcined at 500 °C for 4 h without a catalyst washing process.

4.3. Ethanol Steam Reforming Process

Figure 8 shows the schematic diagram of ESR process used in this work. The catalysts were tested in a quartz tubular reactor with an inner diameter of 1 cm to evaluate the gas production from ESR. To minimize the temperature gradients inside the catalyst bed, the catalyst (0.1 g) was mixed with fine quartz powder (0.4 g, Sigma-Aldrich, St. Louis, USA) then packed between quartz wool in the reactor. The catalyst reduction process was conducted using 50 vol % H₂ (99.99% purity, Linde Thailand Pub Co., Ltd., Samut Prakan, Thailand) balanced in Ar (99.999% purity, Linde Thailand Pub Co., Ltd.) at a total flow rate of 50 mL·min⁻¹ at 600 °C for 1 h. Then, the reactor was purged with 50 mL·min⁻¹ Ar at 600 °C for 30 min to remove excess H₂. Carrier gas (Ar) at the flow rates of 30 mL·min⁻¹ and 10 mL·min⁻¹ were flowed into saturators containing water at 98.4 °C, and ethanol at 80 °C, respectively. Feed reactant was a mixture of ethanol to water with the molar ratio of 1:3. The catalyst activity tests were performed at 550 °C and 650 °C in a continuous mode for 2 h and 30 h for the stability test. The product gas was sent directly to an auto sampling unit of the Gas Chromatography with Thermal Conductivity Detector (GCMS-2010 Ultra, Shimadzu Corporation, Kyoto, Japan) to determine the composition of the gas products. The H₂, CO₂ and CO production rates were calculated by measuring the gas product flow rate and multiplying it with the mole percentage of each gas component determined from GC. The values corresponded to average values during 2 h reaction runs.

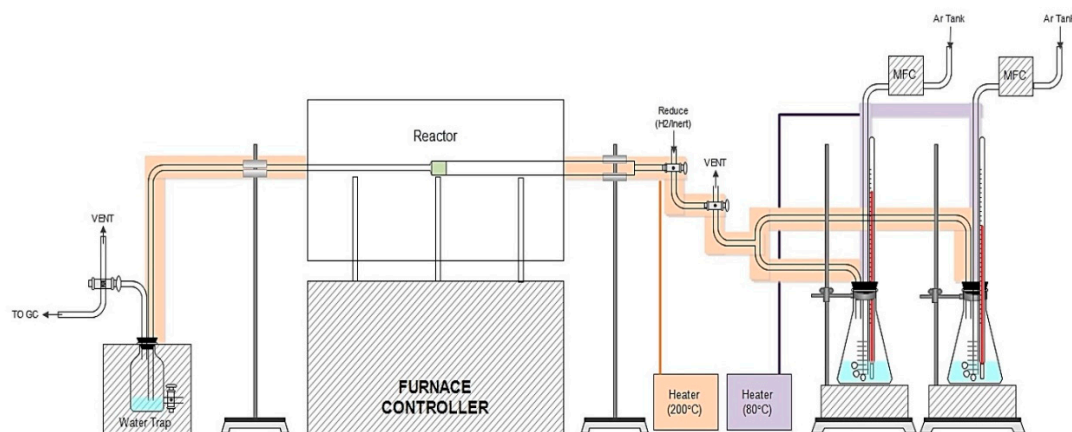


Figure 8. Schematic diagram of the ethanol steam reforming (ESR) process.

4.4. Support Characterization

X-ray diffraction technique (XRD, X'Pert PRO diffractometer, PANalytical, Almelo, Netherlands) with Cu $K\alpha_1$ radiation at 40 kV and 45 mA, 23° – 73° 2-theta, 0.02° step size, and 0.5 s step time was used to characterize the structures of the supports. JADE software (Materials Data, Inc., Livermore, CA, USA) was used to determine the lattice constant of the Al_2O_3 structure from peak deconvolution on the XRD pattern of supports prior, which corresponded to the diffraction angles at around 46 and 67 degrees, with the highest diffraction planes of (4 0 0) and (4 4 0) in the diffractogram. Brunauer, Emmett and Teller (BET) technique (Autosorp-1C, Quantachrome, FL, USA) was used to evaluate the surface areas, the pore volumes, and the pore diameters of the supports. X-ray photoelectron spectroscopy analysis (XPS) acquired with Kratos Axis Supra XPS spectrometer using a monochromated Al $K\alpha$ x-ray source operated at 450 mA and 15 kV was used to determine Al 2p and Ce 3p XPS spectra of Al_2O_3 and CeO_2 – Al_2O_3 supports.

4.5. Catalyst Characterization

CO chemisorption by a pulse injection technique was conducted using 10 vol % CO in He (Linde Thailand Pub Co., Ltd., Samut Prakan, Thailand). The chemisorption spectra of the catalysts were subtracted by the baseline taken from CO pulse chemisorption on the corresponding supports to determine Ni dispersion and Ni surface area on the catalysts (CO-pulse, BELCAT-B, BEL Japan Inc., Osaka, Japan). SEM-EDS (JSM 7800F, JEOL Japan Inc., Japan) was used to determine the distribution of Ce in the Ni/ CeO_2 – Al_2O_3 catalysts. The Ni contents on the catalysts were determined using inductively coupled plasma optical emission spectrometry (ICP-OES, OptimaTM 8300, PerkinElmer, MA, USA) to verify Ni contents in each catalyst. The catalysts were digested with 65 vol % HNO_3 solution to obtain the Ni catalyst solutions using the microwave digestion technique. The catalyst solutions were diluted 50 times with deionized water to obtain the Ni contents in the catalyst solutions in the range of $mg \cdot L^{-1}$. The Ni contents in the catalyst solutions were determined using the MultiElement Calibration Standard 2 (PerkinElmer Plus, USA), with a working range of 0.1 – $100 mg \cdot L^{-1}$ for Ni. Temperature Programmed Oxidation (TPO) using 10 vol % O_2 in He (Linde Thailand Pub Co., Ltd.) was also conducted using the Chemisorption Catalyst analyzer (BELCAT-B, BEL Japan Inc., Japan). The mixed gas was fed at $50 cm^3/min$ with temperature ramping rate of $10^\circ C \cdot min^{-1}$ to $900^\circ C$ and the amount of CO_2 produced during combustion was recorded to determine the amount of coke formation on the used catalyst after reaction. X-ray photoelectron spectroscopy analysis (XPS) acquired with Kratos Axis Supra XPS spectrometer using a monochromated Al $K\alpha$ x-ray source operating at 15 mA and 15 kV was used to determine Ni 2p XPS spectra for Ni on CeO_2 – Al_2O_3 supports. The XPS peak pattern of each catalyst was observed to determine the oxidation state of Ni of different catalysts.

Author Contributions: Conceptualization, P.V., P.T., L.L. and S.C.; methodology, P.V. and P.T.; investigation, P.V., S.A. and S.K.; writing—original draft preparation, P.V., S.A. and S.K.; writing—review and editing, P.T., L.L. and S.C.; supervision, P.T. All authors have read and agreed to the published version of the manuscript.

Funding: This research received no external funding.

Acknowledgments: This study was supported by Thammasat University Research Fund, Contact No. TUFT 067/2563 and the thesis support from the Scholarship for Excellent Thai Student (ETS), Sirindhorn International Institute of Technology (SIIT), Thammasat University (TU). This work was also supported by the National Science and Technology Development Agency Thailand (NSTDA) and Center of Scientific Equipment for Advanced Research, Thammasat University (TUCSEAR).

Conflicts of Interest: The authors declare no conflict of interest.

References

1. Benito, M.; Sanz, J.; Isabel, R.; Padilla, R.; Arjona, R.; Daza, L. Bio-ethanol steam reforming: Insights on the mechanism for hydrogen production. *J. Power Sources* **2005**, *151*, 11–17. [[CrossRef](#)]
2. Ogo, S.; Sekine, Y. Recent progress in ethanol steam reforming using non-noble transition metal catalysts: A review. *Fuel Process. Technol.* **2020**, *199*, 106238. [[CrossRef](#)]
3. Arslan, A.; Doğu, T. Effect of calcination/reduction temperature of Ni impregnated CeO₂–ZrO₂ catalysts on hydrogen yield and coke minimization in low temperature reforming of ethanol. *Int. J. Hydrog. Energy* **2016**, *41*, 16752–16761. [[CrossRef](#)]
4. Kumbilieva, K.; Petrov, L.; Alhamed, Y.A.; Alzahrani, A. Reaction Mechanism and Deactivation Modes of Heterogeneous Catalytic Systems. *Chin. J. Catal.* **2011**, *32*, 387–404. [[CrossRef](#)]
5. Vicente, J.; Ereña, J.; Montero, C.; Azkoiti, M.J.; Bilbao, J.; Gayubo, A.G. Reaction pathway for ethanol steam reforming on a Ni/SiO₂ catalyst including coke formation. *Int. J. Hydrog. Energy* **2014**, *39*, 18820–18834. [[CrossRef](#)]
6. Ni, M.; Leung, D.Y.; Leung, M.K. A review on reforming bio-ethanol for hydrogen production. *Int. J. Hydrog. Energy* **2007**, *32*, 3238–3247. [[CrossRef](#)]
7. Kugai, J.; Velu, S.; Song, C. Low-temperature reforming of ethanol over CeO₂-supported Ni-Rh bimetallic catalysts for hydrogen production. *Catal. Lett.* **2005**, *101*, 255–264. [[CrossRef](#)]
8. Cavallaro, S. Low-temperature reforming of ethanol over CeO₂-supported Ni-Rh bimetallic catalysts for hydrogen production. *Energy Fuels* **2000**, *14*, 1195–1199. [[CrossRef](#)]
9. Auprêtre, F.; Descorme, C.; Duprez, D. Bio-ethanol catalytic steam reforming over supported metal catalysts. *Catal. Commun.* **2002**, *3*, 263–267. [[CrossRef](#)]
10. Montero, C.; Remiro, A.; Valle, B.; Oar-Arteta, L.; Bilbao, J.; Gayubo, A.G. Origin and Nature of Coke in Ethanol Steam Reforming and Its Role in Deactivation of Ni/La₂O₃– α -Al₂O₃ Catalyst. *Ind. Eng. Chem. Res.* **2019**, *58*, 14736–14751. [[CrossRef](#)]
11. Sepehri, S.; Rezaei, M. Ce promoting effect on the activity and coke formation of Ni catalysts supported on mesoporous nanocrystalline γ -Al₂O₃ in autothermal reforming of methane. *Int. J. Hydrog.* **2017**, *42*, 11130–11138. [[CrossRef](#)]
12. Das, S.; Ashok, J.; Bian, Z.; Dewangan, N.; Wai, M.; Du, Y.; Borgna, A.; Hidajat, K.; Kawi, S. Silica–Ceria sandwiched Ni core–shell catalyst for low temperature dry reforming of biogas: Coke resistance and mechanistic insights. *Appl. Catal. B* **2018**, *230*, 220–236. [[CrossRef](#)]
13. Pu, J.; Luo, Y.; Wang, N.; Bao, H.; Wang, X.; Qian, E.W. Ceria-promoted Ni@Al₂O₃ core-shell catalyst for steam reforming of acetic acid with enhanced activity and coke resistance. *Int. J. Hydrog.* **2018**, *43*, 3142–3153. [[CrossRef](#)]
14. Kathiraser, Y.; Wang, Z.; Ang, M.; Mo, L.; Li, Z.; Oemar, U.; Kawi, S.-. Highly active and coke resistant Ni/SiO₂ catalysts for oxidative reforming of model biogas: Effect of low ceria loading. *J. CO₂ Util.* **2017**, *19*, 284–295. [[CrossRef](#)]
15. Fard, A.A.; Arvaneh, R.; Alavi, S.M.; Bazyari, A.; Valaei, A. Propane steam reforming over promoted Ni–Ce/Mg Al₂O₄ catalysts: Effects of Ce promoter on the catalyst performance using developed CCD model. *Int. J. Hydrog.* **2019**, *44*, 21607–21622. [[CrossRef](#)]
16. Sharma, Y.C.; Kumar, A.; Prasad, R.; Upadhyay, S.N. Ethanol steam reforming for hydrogen production: Latest and effective catalyst modification strategies to minimize carbonaceous deactivation. *Renew. Sustain. Energy Rev.* **2017**, *74*, 89–103. [[CrossRef](#)]

17. Kumar, P.; Sun, Y.; Idem, R.O. Nickel-Based Ceria, Zirconia, and Ceria–Zirconia Catalytic Systems for Low-Temperature Carbon Dioxide Reforming of Methane. *Energy Fuels* **2007**, *21*, 3113–3123. [[CrossRef](#)]
18. Ebiad, M.A.; El-Hafiz, D.R.A.; Elsalamony, R.A.; Mohamed, L.S. Ni supported high surface area CeO₂–ZrO₂ catalysts for hydrogen production from ethanol steam reforming. *RSC Adv.* **2012**, *2*, 8145–8156. [[CrossRef](#)]
19. Pacchioni, G. Oxygen Vacancy: The Invisible Agent on Oxide Surfaces. *ChemPhysChem* **2003**, *4*, 1041–1047. [[CrossRef](#)]
20. Fujiwara, M.; Chie, K.; Sawai, J.; Shimizu, D.; Tanimoto, Y. On the Movement of Paramagnetic Ions in an Inhomogeneous Magnetic Field. *J. Phys. Chem. B* **2004**, *108*, 3531–3534. [[CrossRef](#)]
21. Wu, Y.-J.; Santos, J.; Li, P.; Yu, J.-G.; Cunha, A.F.; Rodrigues, A.E. Simplified kinetic model for steam reforming of ethanol on a Ni/Al₂O₃ catalyst. *Can. J. Chem. Eng.* **2014**, *92*, 116–130. [[CrossRef](#)]
22. Zhou, Y.; Perket, J.M.; Crooks, A.B.; Zhou, J. Effect of Ceria Support on the Structure of Ni Nanoparticles. *J. Phys. Chem. Lett.* **2010**, *1*, 1447–1453. [[CrossRef](#)]
23. Chang, K.-T.; Weng, C.-I. An investigation into the structure of aqueous NaCl electrolyte solutions under magnetic fields. *Comput. Mater. Sci.* **2008**, *43*, 1048–1055. [[CrossRef](#)]

Publisher’s Note: MDPI stays neutral with regard to jurisdictional claims in published maps and institutional affiliations.



© 2020 by the authors. Licensee MDPI, Basel, Switzerland. This article is an open access article distributed under the terms and conditions of the Creative Commons Attribution (CC BY) license (<http://creativecommons.org/licenses/by/4.0/>).